Digital Signal Processing 23 (2013) 1856–1866

Contents lists available at SciVerse ScienceDirect

Digital Signal Processing

www.elsevier.com/locate/dsp

Automatic contrast enhancement of low-light images based on local statistics of wavelet coefficients

Artur Łoza [a,*], David R. Bull [b], Paul R. Hill [b], Alin M. Achim [b]

[a] Department of Electrical and Computer Engineering, Khalifa University of Science, Technology and Research, United Arab Emirates
[b] Department of Electrical and Electronic Engineering, University of Bristol, UK

ARTICLE INFO

Article history:
Available online 17 June 2013

Keywords:
Wavelets
Statistical modelling
Image and video contrast enhancement
Denoising

ABSTRACT

This paper describes a new method for contrast enhancement in images and image sequences of low-light or unevenly illuminated scenes based on statistical modelling of wavelet coefficients of the image. A non-linear enhancement function has been designed based on the local dispersion of the wavelet coefficients modelled as a bivariate Cauchy distribution. Within the same statistical framework, a simultaneous noise reduction in the image is performed by means of a shrinkage function, thus preventing noise amplification. The proposed enhancement method has been shown to perform very well with insufficiently illuminated and noisy imagery, outperforming other conventional methods, in terms of contrast enhancement and noise reduction in the output data.

1. Introduction

Night vision sensors, such as image intensifiers and forward looking infrared sensors are frequently used for capturing nighttime imagery. These can also be complemented by visible range sensors. The resulting image quality however, can be extremely poor, with poor contrast, resolution, limited dynamic range and graininess. Dynamic range in digital images and videos can be affected by various factors: intensity of light in the scene (nighttime, weather conditions, insufficient lighting), non-uniform exposure (shadows), too short shutter cycle of the camera and too low dynamic range of the sensor or the display device. In all cases, low dynamic range distorts the contrast in the image and results in high noise levels. This often leads to confusion of objects and textures, the inability to segment them, and visual illusions, resulting in disorientation, user fatigue, poor detection and classification performance of humans and computer algorithms. In order to improve the visual quality of the image for human or machine vision it is necessary to modify its intensity values and, in particular, to enhance its contrast.

The most commonly used image Contrast Enhancement (CE) methodologies include grey-level transformations by means of non-linear functions (logarithm [1], power-law [2], gamma function [3], etc.), histogram-based techniques [4–15] (see [13] for a comprehensive review), contrast-tone optimisation [16], non-linear quadratic filtering [17], and methods operating in the frequency domain, such as the homomorphic filter [18]. Often, a combination of several techniques gives improved results, for example logarithmic pixel transformation combined with morphological operations used to determine the base intensity [19]. Although the majority of grey-level transformation methods operate in the spatial domain, several authors have in recent years advocated the use of wavelets and other multiscale (curvelets [20,21], steerable pyramids [22], etc.) or discrete cosine representation [23] for this purpose. The advantage of using these representations is their ability to analyse and modify image features based on their spatial-frequency content at different resolutions. Early work on CE in the wavelet domain has been reported in [24] where a parametrised hyperbolic function was applied to the gradient of wavelet coefficients and in [25] where echocardiographic images were both denoised and enhanced by applying a combination of sigmoid functions to high-pass coefficients. Many other authors have reported successful enhancement with other parametrised functions. Specifically these include: scaling based on second derivative-like contrast measure [26] or applied to multiscale gradient [27], the gamma function applied to either curvelet coefficients [20] or to steerable pyramid [22], piecewise-linear functions [28–30], or a combination of sigmoid curves [21] applied to curvelet coefficients, a hyperbolic tangent weighted by a Gaussian applied to contourlet coefficients [31–33]. Multiscale CE by fusion of multimodal images was first reported in [34]. The multiscale-based CE techniques have been shown to outperform other conventional techniques, such as gamma correction and histogram stretching or equalisation in terms of visual impression.

When using parametrised CE functions, a common issue is the choice of suitable parameters that have to be estimated in order to compute an optimal transfer function for a particular image

* Corresponding author.
E-mail addresses: Artur.Loza@kustar.ac.ae (A. Łoza), Dave.Bull@bristol.ac.uk (D.R. Bull), Paul.Hill@bristol.ac.uk (P.R. Hill), Alin.Achim@bristol.ac.uk (A.M. Achim).

1051-2004/$ – see front matter
http://dx.doi.org/10.1016/j.dsp.2013.06.002

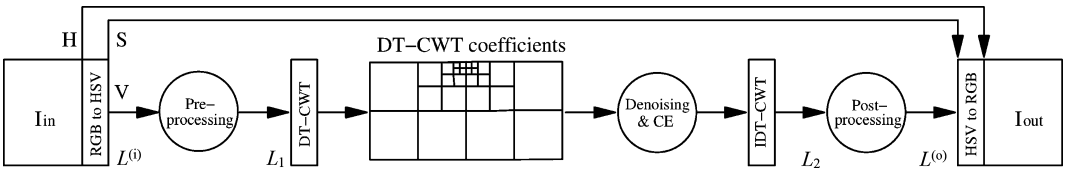

Fig. 1. The data flow of the proposed image enhancement method. $L^{(i)}$, L_1, L_2, $L^{(o)}$ correspond to input, pre-processed, enhanced and output luminance, respectively.

[9,10,15]. The practise often encountered in the literature is to determine the parameters, for example, the boosting gain and interval and the function shape parameters, based on an off-line test on a representative set of images [7,28,22,31,8,11,35,12]. Notable exceptions are the methods that make some parameters dependent on the statistics of the wavelet subband, or derive them from assumed general characteristics of 'natural' or 'an ideal' image [20,22,28]. It seems, however, that a large degree of heuristic manipulation is still necessary when establishing direct relationship between the parameter and the signal characteristics, and eventually various user-defined parameters or multipliers are utilised. The need for automated CE procedure becomes even more obvious when processing video sequences, where off-line estimation may not be possible. When enhancing videos or low-light image sequences frame-by-frame, the use of aforementioned methods may cause a flicker effect in scenes with rapid dynamic changes. This issue, although occasionally acknowledged by various authors is rarely addressed properly. Proposed solutions include averaging the gain of the output image over several frames [8,35] with the weights determined by trial and error, conditioning the current histogram on the histogram of the previous frame [11] and modelling the luminance change adaptation of the human eye using exponential decay function [36]. As a result none of these methods fully guarantees the absence of flicker in a wide range of videos.

In this work, the design of a fast and simple CE algorithm that operates on a wide range of imagery without the need for user intervention is presented. The algorithm enhances contrast in images and image sequences adaptively, and, as opposed to global approaches, estimates the parameters based on local statistics of the wavelet coefficients of an image. Moreover, the amplification of the noise in the image is avoided by simultaneously denoising the wavelet coefficients based on the same statistical assumptions. In order to address the flicker problem in the enhanced video, we derive a simple normalisation scheme where the change due to normalisation is limited by the perceptually acceptable contrast change derived from a Hue-Saturation-Value (HSV) model. When evaluating the enhancement results, several computational quality measures are used in a novel manner alongside with the usually utilised subjective visual observation.

The remaining part of this paper is organised as follows. The proposed enhancement method is described in detail in Section 2, where a new contrast measure and the statistical basis for image denoising and contrast enhancement are given. The performance of the method is evaluated on a set of images and is compared with other CE techniques in Section 3. Finally, Section 4 presents the conclusions of the study.

2. Contrast enhancement method

The main goal of the proposed image and video enhancement method is to improve readability of the imagery recorded in low-light or uneven exposure conditions. Such images are often characterised by high noise levels and very uneven spatial intensity distributions. Generally speaking, in order to enhance a low-light image, the low and middle intensity pixels should be boosted, while the high intensity pixels should be either left unchanged or compressed. Special care should be taken when boosting the small intensity pixels, so that noise in the image is not amplified. Ideally, the contrast in the image should be enhanced locally, while maintaining globally balanced intensity in the image. The data flow of the proposed enhancement method is shown in Fig. 1 and explained in the following paragraphs. Throughout this paper the term "image" will be used to refer both to a still image and a frame in a video (or in an image sequence) and whenever necessary the distinction between the two will be made.

2.1. RGB to HSV transform

When colour images are processed, instead of enhancing each colour channel separately, the Red–Green–Blue (RGB) representation is converted to the HSV colour space and only the V channel is further processed. This approach allows dimensionality reduction of the processed data and close reconstruction of the original colours in the output image (processing RGB channels separately often leads to significantly distorted colours in the output image). Thus the V component is treated as a grey-scale image during subsequent processing. The three HSV channels are obtained as follows [37]:

$$V = \max(R, G, B), \tag{1}$$

$$S = \begin{cases} 0 & \text{if } V = 0, \\ \frac{C}{V} & \text{otherwise}, \end{cases} \tag{2}$$

$$H = \begin{cases} \frac{G-B}{S} & \text{if } R = V, \\ 2 + \frac{B-R}{S} & \text{if } G = V, \\ 4 + \frac{R-G}{S} & \text{if } B = V, \end{cases} \tag{3}$$

where C (chroma) is calculated as follows

$$C = \begin{cases} 1 & \text{if } V = \min(R, G, B), \\ V - \min(R, G, B) & \text{otherwise.} \end{cases} \tag{4}$$

2.2. Pre-processing

The pixels of images or videos recorded in low-light scenarios usually are characterised by a very low dynamic range, not matching that of the sensing and/or display device used. Hence, it is necessary to initially normalise the images or video frames so that the full dynamic range is utilised. For still images it is sufficient to linearly scale pixels to fit the full [0 1] range, by applying the following transform:

$$L_1(k) = \frac{L^{(i)}(k) - \min\{L^{(i)}(k)\}}{\max\{L^{(i)}(k) - \min\{L^{(i)}(k)\}\}}, \tag{5}$$

where $L^{(i)}(k)$ is the input video frame at time instant k and the max and min operators are used to obtain the maximum and minimum luminance in given frame, respectively. However, when dealing with videos, the dynamic range may change rapidly from frame to frame, for example as a result of a bright or dark object entering the scene, a sudden change in the light conditions (e.g. bright lights turned on), or sudden adjustments of the camera's sensitivity. Thus normalising each frame based purely on its current full dynamic range or $\max\{L^{(i)}(k)\}$ (the image can be normalised to have constant $\min\{L^{(i)}(k)\}$) may cause undesirable flicker in the

enhanced video that may distract or tire the human operator. Examples of such occurrences are shown in Fig. 5(a).

Rapid changes of brightness in the enhanced video can be avoided by introducing temporal dependency in the normalisation. In this work, it is proposed to limit the amount of the contrast frame-to-frame change to the value derived from perceptual contrast discrimination threshold. For the purposes of normalisation, the contrast in the current frame, k, is defined as follows

$$W(k) = \frac{\bar{L}^{(\mathrm{i})}(k) - \min\{L^{(\mathrm{i})}(k)\}}{\min\{L^{(\mathrm{i})}(k)\} + 1}. \tag{6}$$

The use of the mean luminance value $\bar{L}^{(\mathrm{i})}$ instead of $\max\{L^{(\mathrm{i})}(k)\}$ ensures that the high value luminance outliers have limited effect on the contrast estimate. The base intensity can be adjusted to be constant for all frames $\min\{L^{(\mathrm{i})}(k)\} = 0$ and therefore from (6)

$$\begin{aligned}\Delta W(k) &= W(k+1) - W(k) = \bar{L}^{(\mathrm{i})}(k+1) - \bar{L}^{(\mathrm{i})}(k) \\ &= \Delta\bar{L}^{(\mathrm{i})}(k).\end{aligned} \tag{7}$$

It has been shown in [38] that the Human Visual System (HVS) detection thresholds ΔW_{thr} (from one frame to another) for the full range of visible contrast (the measurements published in [39]) can be modelled by fitting a continuous function to the empirical data:

$$\Delta W_{\mathrm{thr}}(k) = 0.0928 W(k)^{1.08} + 0.0046 W(k)^{-0.183}. \tag{8}$$

The rescaling of the intensity range in the frame $k+1$ that causes the change of contrast $\Delta W(k) = \Delta W_{\mathrm{thr}}(k)$ is achieved by scaling the image by a factor g calculated as follows:

$$g = 1 + \operatorname{sign}\big(\Delta\bar{L}^{(\mathrm{i})}(k)\big)\frac{\Delta W_{\mathrm{thr}}}{\bar{L}^{(\mathrm{i})}(k)}. \tag{9}$$

It is proposed that, in case of processing a video, the first frame is normalised according to (5) and then the following frames are adjusted using (9).

2.3. Dual-tree complex wavelet transform

Preferably, features appearing at particular scales should be enhanced selectively, and the wavelet transform enables us to achieve this goal at very small computational expense resulting in improved performance. The pre-processed image is hence transformed into the multi-resolution domain. In this work, the Dual-Tree Complex Wavelet Transform (DT-CWT) [40] is used,[1] a redundant multiscale representation, characterised by near shift-invariance and improved directional selectivity over the conventional Discrete Wavelet Transform. Near shift-invariance is achieved at a small computational expense resulting from redundancy in the representation (6 evenly spaced orientations represented by the complex coefficients). Following the recommendations in [41,42] and an experimental verification, it was decided to use *AntonB* filters with decomposition levels chosen depending on the size of the image according to the following formula: $J = \lfloor(\log_2 \min\{N_w, N_h\})\rfloor - 4$, where N_w and N_h are the width and height of the image, respectively. For the images in our database J typically takes on values 4 or 5.

2.4. Denoising with Cauchy priors

As mentioned in the introduction to Section 2, when performing contrast enhancement the amplification of the noise present in low-light images should be avoided. In our work this is achieved by combining contrast enhancement with denoising operation. The wavelet coefficients are denoised by applying the shrinkage functions derived as Maximum A Posteriori (MAP) estimators $\hat{w}_j$ of noisy wavelet coefficient x_j at the decomposition level j corrupted by white Gaussian noise n: $x_j = w_j + n$, $n \sim N(0, \sigma_n)$. The evidence from previous studies (e.g. [43,44] and references therein), indicates that the wavelet coefficients of images (w_j) frequently follow a model that deviates significantly from the Gaussian model and can be more accurately modelled by symmetric α stable (SαS) models. A visual example of how the underlying distribution of the images from our dataset deviates from the normal distribution is shown in Fig. 2(a). The circles in the plots show the empirical probability versus the data values for each point in the sample. The circles are in curves that do not follow the straight Gaussian lines and thus, the normality assumption is violated for all these data. On the other hand, the low-amplitude coefficients following the normal model (the straight line, Fig. 2(a)) support the Gaussian noise assumption.

The appeal of SαS distributions as a statistical signal model is based on two important theoretical points [45,46]. Firstly, stable random variables satisfy the stability property which states that linear combinations of jointly stable variables are indeed stable. The word *stable* is used because the shape of the distribution is unchanged (or stable) under such linear combinations. Secondly, stable processes arise as limiting processes of sums of independent and identically distributed (iid) random variables via the generalised central limit theorem. Actually, the *only* possible non-trivial limit of normalised sums of iid terms is stable. The SαS distribution is best defined by its characteristic function (i.e. the Fourier transform of the pdf)

$$\varphi(\omega) = \exp\big(i\delta\omega - \gamma|\omega|^{\alpha}\big), \tag{10}$$

where ω represents frequency, i is the imaginary unit, α is the *characteristic exponent*, taking values $0 < \alpha \leqslant 2$, δ $(-\infty < \delta < \infty)$ is the *location parameter* ($\delta = 0$ in our work), and $\gamma > 0$ is the *dispersion* parameter that determines the spread of the distribution. The characteristic exponent, α, determines the shape of the distribution. The smaller α is, the heavier the tails of the SαS density function. Gaussian processes are stable processes with $\alpha = 2$, while Cauchy processes result when $\alpha = 1$. In fact, no closed-form expressions for the general SαS pdf are known except for the Gaussian and the Cauchy members. The univariate probability distribution for the latter case is written as

$$p(w_j) = \frac{\gamma}{\pi(w_j^2 + \gamma^2)}. \tag{11}$$

Although the SαS density function behaves approximately like a Gaussian density function near the origin, its tails decay at a lower rate [45]. Specifically, while the Gaussian density function has exponential tails, the stable densities have algebraic tails, that is, $P(W > w) \sim c_\alpha w^{-\alpha}$ as $w \to \infty$, where $c_\alpha = \Gamma(\alpha)(\sin(\pi\alpha/2))/\pi$. Fig. 2(b) shows the tail behaviour of several SαS densities including the Cauchy and the Gaussian and Figs. 2(c)–2(d) compare the fit of the density functions to the empirical distributions of wavelet coefficients of selected images. Note that whereas the SαS pdf provides a better fit to both the mode and the tails of the empirical density of the actual data, its special case, the Cauchy model, offers the best trade-off between flexibility in capturing the tails (and the shape in general) of a distribution and mathematical tractability through the availability of a closed-form expression for its pdf. For more detailed analysis of the images the reader is referred to [43].

In order to account for interscale dependencies of wavelet coefficients the bivariate statistical model of the wavelet coefficients is used, written as

[1] DT-CWT code accessed at http://eeweb.poly.edu/iselesni/WaveletSoftware/ has been adopted in this work.

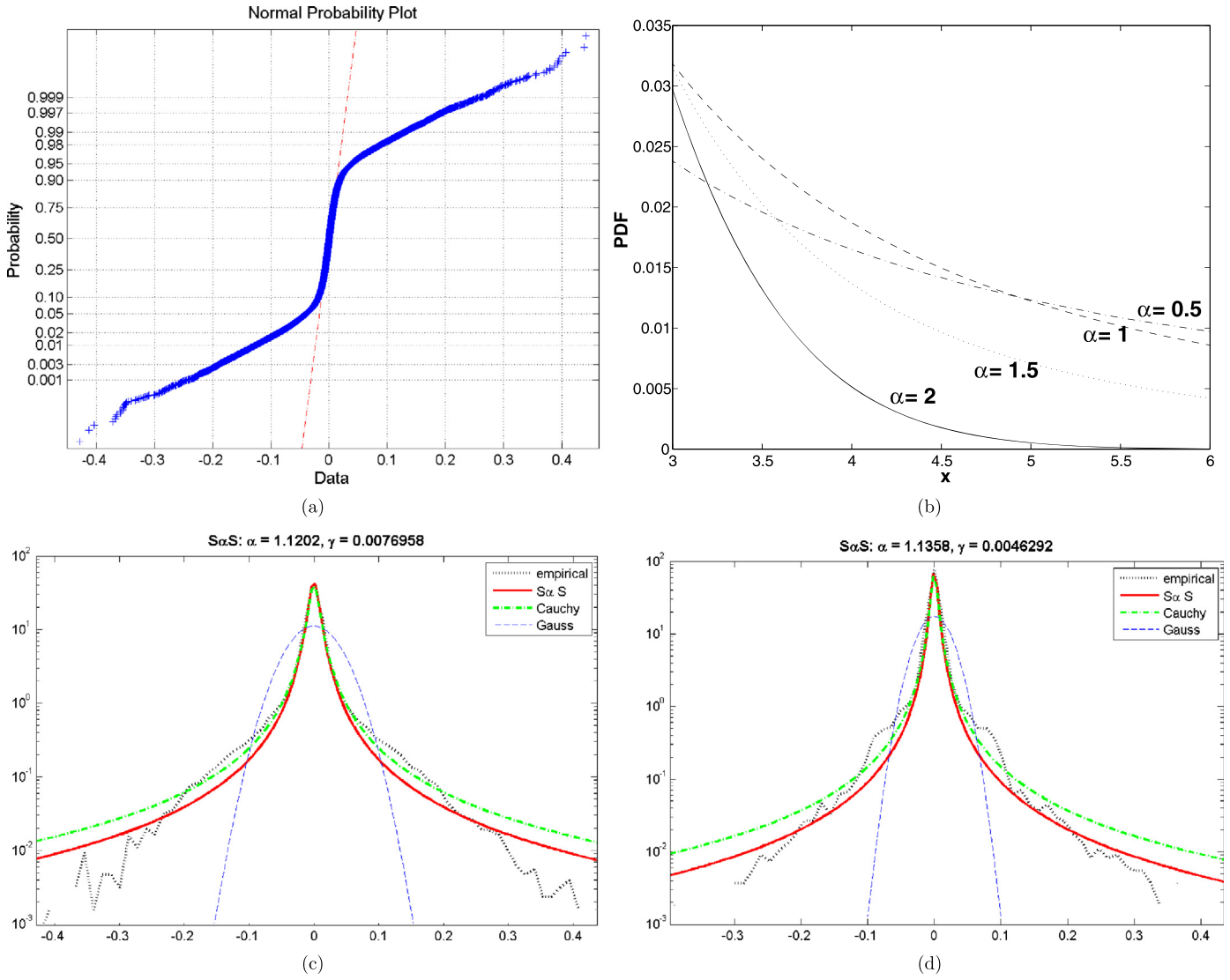

Fig. 2. Modelling of wavelet coefficients of an image: (a) normal probability plot of *Landrover* image – empirical data (circles), theoretical Gaussian data (straight line), (b) tail behaviour of the Symmetric Alpha-Stable (SαS) probability density functions for $\alpha = 0.5$, 1.0 (Cauchy), 1.5, and 2.0 (Gaussian), for the dispersion parameter $\gamma = 1$, (c)–(d) the fit of the empirical distribution (dotted line) of wavelet coefficients of the *Landrover* and *Greenwich* images, respectively, with the SαS (solid line), Cauchy (dash-dotted line) and the Gaussian (dashed line) density functions.

$$p(w_j, w_{j+1}) = \frac{\gamma}{2\pi (w_j^2 + w_{j+1}^2 + \gamma^2)^{\frac{3}{2}}} \tag{12}$$

where w_j and w_{j+1} are the current and parent wavelet coefficients on the decomposition level j and $j+1$, respectively. The MAP estimate of the wavelet coefficient is obtained from the following shrinkage relationship as derived in [44]:

$$\hat{w}_j = A_d(x_j) x_j, \tag{13}$$

where $A_d(x_j) = \frac{1}{3} + s + t$,

$$s = \sqrt[3]{-\frac{q}{2} + \sqrt{\frac{p^3}{27} + \frac{q^2}{4}}}, \qquad t = \sqrt[3]{-\frac{q}{2} - \sqrt{\frac{p^3}{27} + \frac{q^2}{4}}}$$

and

$$p = \frac{(\gamma^2 + 3\sigma_n^2)}{x_j^2 + x_{j+1}^2} - \frac{1}{3}, \qquad q = -\frac{2}{27} + \frac{1}{3}\frac{\gamma^2 + 3\sigma_n^2}{x_j^2 + x_{j+1}^2} - \frac{\gamma^2}{x_j^2 + x_{j+1}^2}.$$

The parameter γ is estimated based on the empirical characteristic function [47] as follows:

$$\hat{\gamma} = -\frac{\log \hat{\varphi}^2(\omega) - \sigma_n^2 |\omega|^2}{2|\omega|}, \tag{14}$$

where $\hat{\varphi}(\omega) = \frac{1}{M}\sum_{m=1}^{M} \exp(i\omega x_j(m))$ is the sample estimate of empirical characteristic function $\hat{\varphi}(\omega)$ from M wavelet coefficients and $\hat{\gamma}$ is obtained as the average of the estimates corresponding to several possible choices of $\omega = \frac{2\pi k}{K}$ where $k = 2, 3, 4$ and $K = 512$. The noise variance, σ_n^2, required to compute the shrinkage functions, is obtained from the observed data by computing the Median Absolute Deviation (MAD) of the detail coefficients at the first decomposition level of a wavelet decomposition [48,49]

$$\hat{\sigma}_n = \frac{MAD(X_1)}{0.6745}. \tag{15}$$

2.5. Contrast enhancement

We begin the design of our CE routine by defining the contrast measure. Various contrast measures have been proposed in the literature (see [1,38] for details and a comparison of different contrast measures), most commonly being:

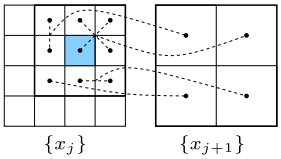

Fig. 3. Illustration of the correspondence between the wavelet coefficients on a child (fine scale), j, and the parent (coarse scale) decomposition level, $j+1$. The coefficients are contained within a local window (thick-line) centred around the reference coefficient (shaded).

$$C_s = \frac{\max\{L\}}{\min\{L\}} \quad \text{simple contrast,}$$

$$C_W = \frac{\Delta L}{\min\{L\}} \quad \text{Weber fraction,}$$

$$C_l = \log_{10}\left(\frac{\max\{L\}}{\min\{L\}}\right) \quad \text{logarithmic ratio,}$$

$$C_M = \frac{|\max\{L\} - \min\{L\}|}{\max\{L\} + \min\{L\}} \quad \text{Michelson contrast,}$$

where L stands for intensity (luminance) of the image pixel. These measures have been originally designed for the spatial domain and are concerned with a pixel-to-neighbourhood relationship. When applied in a transform domain, however, they often result in an unreliable measurement, especially for high-pass complex image content that can be regarded as features (as opposed to isolated pixels) with the mean intensity removed out by low-pass filtering. Thus, in this work, a new contrast measure is proposed, suitable for wavelet transform domain, defined in terms of the local dispersion of the wavelet coefficients

$$C(x_j) = \frac{\max\{\hat{\gamma}_j(x_j)\}}{\hat{\gamma}_j(x_j)}. \tag{16}$$

The measure (16) is calculated by means of (14) within a 3×3 multiscale sliding window centred around each coefficient x_j, as illustrated in Fig. 3. Contrast $C(x_j)$ is computed with respect to the maximum dispersion in the current wavelet subband, $\max\{\hat{\gamma}_j\}$, $x_j \in X_j$; its estimate serves as a reference value towards which the wavelet coefficients are boosted in order to obtain the desired contrast. The bivariate statistical model of the wavelet coefficients (12), provides the basis for both denoising and contrast enhancement and accounts for interscale dependencies of wavelet coefficients, assigning more importance to persistent multiscale patterns when both denoising and enhancing the contrast of the image.

The local contrast values are used to adjust the corresponding wavelet coefficients by means of an exponential contrast enhancement function A_c

$$A_c(x_j) = \exp\left(-\frac{1}{C(x_j)}\right) + A_0, \tag{17}$$

where $A_0 = 1 - \exp(-1)$ is a normalisation constant ensuring that the function converges to 1 in the areas of high dispersion. Since shrinkage and enhancement functions are applied sequentially, the enhanced (that is denoised and contrast-enhanced) high-pass wavelet coefficient can be written as a product of the overall enhancement function A_e and the original wavelet coefficient,

$$\hat{w}_j = A_e(x_j)x_j = \big(A_d(x_j)A_c(x_j)\big)x_j, \tag{18}$$

where A_d is the denoising shrinkage function (13) and A_c is the enhancement function calculated as shown in (17) with the use of the high-pass coefficients subband at the corresponding decomposition level. The low-pass coefficients at the final decomposition level are optimised with the use of the Contrast Limited Adaptive Histogram Equalization (CLAHE) [4,5,7]. This popular method divides an image into several non-overlapping regions (in our case width and height not exceeding 8 coefficients). In each region a normalised histogram is calculated and clipped to a specified value (0.03 in our case). The pixels overflowing the clip limit are redistributed across the bins below the clip limit, giving rise to a mapping function. In order to avoid the tiling distortion in the output image, the grey-level mappings are interpolated between the current and neighbouring regions.

Examples of the empirical and theoretical input–output transfer functions corresponding to the denoising A_d, contrast enhancement A_c and combined enhancement functions A_e, as well as the empirical bivariate input–output surfaces are shown in Fig. 4. Specifically, Fig. 4(a) shows the theoretical enhancement curves and displays clearly the non-linearities of denoising (the zeroing zone around the plot origin) and the enhancement operations. Figs. 4(b)–4(c) show the real data input coefficient values plotted against the output coefficients for a first level high-pass subband coefficients extracted from the image *Landrover*.

2.6. Post-processing

In the proposed image enhancement system post-processing consists in logarithmically scaling the image L_2 obtained from the inverse DT-CWT (see Fig. 1) giving the final result the output image $L^{(o)}$

$$L^{(o)} = \frac{\max\{L_2\}}{\log(\max\{L_2\}+1)}\log(L_2+1). \tag{19}$$

The log function approximates the transformation performed by the retina of the HVS and has been widely used to compress dynamic range of images [3,22,38]. The transformation of this type expands the values of dark pixels while compressing the higher-level values of image pixels.

2.7. HSV to RGB transform

Analogously to the pre-processing stage of the system, an HSV to RGB transform is performed, by combining the original H and S components with the modified V component, as shown in Fig. 1 according to the following formula [37]:

$$(R, G, B) = \big(R' + m, G' + m, B' + m\big), \tag{20}$$

where $m = V - C$, C (chroma) is retrieved as $C = VS$ and (R', G', B') is defined as follows

$$\big(R', G', B'\big) = \begin{cases} (C, X, 0) & \text{if } 0 \leqslant H < 1, \\ (X, C, 0) & \text{if } 1 \leqslant H < 2, \\ (0, C, X) & \text{if } 2 \leqslant H < 3, \\ (0, X, C) & \text{if } 3 \leqslant H < 4, \\ (X, 0, C) & \text{if } 4 \leqslant H < 5, \\ (C, 0, X) & \text{if } 5 \leqslant H < 6, \\ (0, 0, 0) & \text{otherwise} \end{cases} \tag{21}$$

with $X = C(1 - |(H \bmod 2)1|)$.

2.8. Summary of the algorithm

The proposed contrast enhancement method for colour images and videos consists of the following steps (cf. Fig. 1):

1. RGB to HSV conversion of the input image I_{in} (1). The H and S channels are unchanged and the $L^{(i)} = \text{V}$ channel is processed further.
2. Normalisation of $L^{(i)}$ according to (5) for still images and according to (9) for video frames.

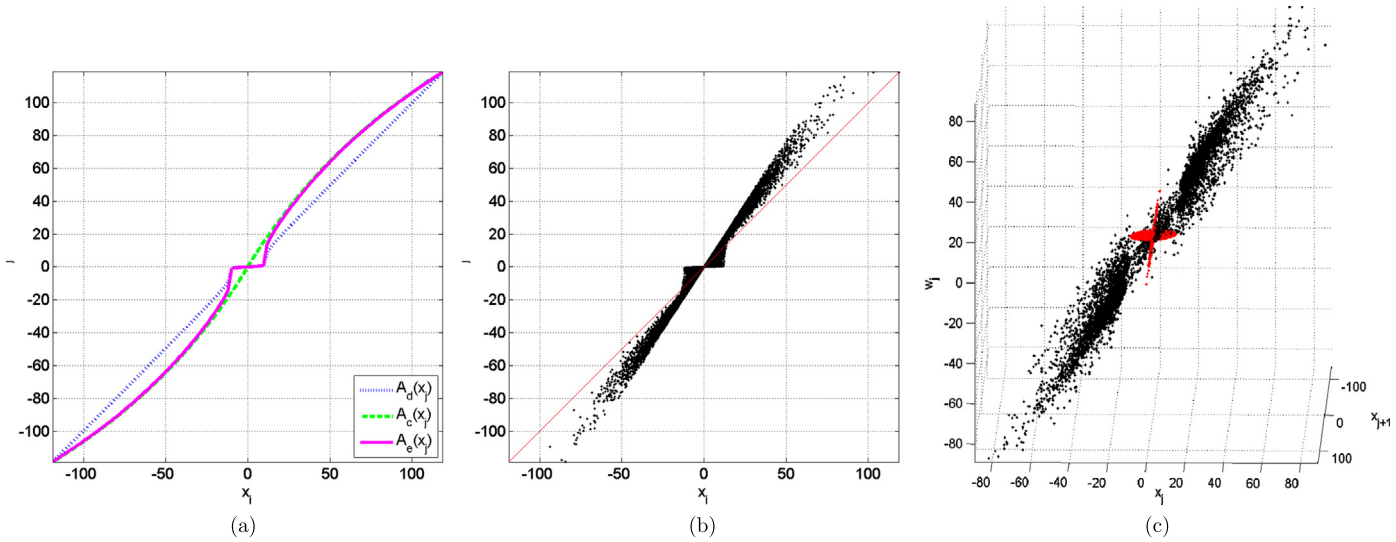

Fig. 4. Examples of input–output plots of image wavelet coefficients $w_j = f(x_j)$ enhanced with the proposed method: (a) examples of interpolated theoretical input–output univariate plots with the dotted, dashed and solid line corresponding to the denoising, contrast enhancement and overall enhancement functions for certain parameter values ($\gamma = 1$, $\sigma_n = 3.5$), (b) empirical univariate plot of enhanced wavelet coefficients computed from wavelet coefficients of the *Landrover* image (decomposition level $j = 1$) displayed as black dots with unity line superimposed, (c) the corresponding bivariate plot with the small-value coefficients (bivariate denoising zone) displayed as red dots for clarity. (For interpretation of the references to color in this figure legend, the reader is referred to the web version of this article.)

3. The resulting normalised image L_1 is transformed to the wavelet domain as described in 2.3.
4. For each wavelet high-pass subband, the denoising function A_d (13) and the enhancement function A_e (17) are computed based on the dispersion estimate $\hat{\gamma}$ (14). The standard deviation of noise $\hat{\sigma}_n$ (15) is estimated only once, at the first decomposition level.
5. The joint denoising and enhancement is performed by applying A_d and A_e to a high-pass wavelet coefficient according to (18).
6. The low-pass coefficients are processed with the use of CLAHE.
7. The modified wavelet coefficients are inverse-transformed back to spatial domain; the resulting image is denoted as L_2.
8. The image L_2 is logarithmically scaled according to (19).
9. Scaled output image $L^{(o)}$ is then combined with the original H and S channels in order to be transformed back to RGB colour space as described in (20); the resulting image is denoted by I_{out}.

3. Experimental results

3.1. Quality measures

The results of the image enhancement method are evaluated in two ways: subjectively (by visual inspection) and objectively (by computing quantitative quality measures). Among the quantitative metrics that have been used, two of them measure a specific type of distortion such as noise and saturation, and two of them are more general image quality measures: entropy [50] and Structural SIMilarity Image Quality Index (SSIM) [51]. In order to evaluate the performance of the methods in terms of noise reduction, we have shown the MAD estimates (15) of the noise standard deviations in the input image, $\sigma_n^{(i)}$, and the enhanced output image, $\sigma_n^{(o)}$. The loss of information resulting from an over-amplification of the image pixels is assessed by *saturation* (S), which measures the percentage of the pixels in the enhanced image that exceed the default image range and thus have to be clipped in order to fit in. The discrete entropy is commonly used to measure the degree of randomness or the average amount of information in the image. It has been extensively used to asses the output of contrast enhancement algorithms as the images with higher contrast and/or more uniform histogram distribution result in higher entropy values [2,11,12]. The entropy H of an image with G discrete grey levels observed with probabilities p_m is written as [52]

$$H = -\sum_{m=1}^{G} p_m \log_2 p_m. \tag{22}$$

For the dataset where the non-corrupted, high-quality reference image is available, an SSIM-based quality measure has been computed. SSIM [51] measures the similarity between the reference image A and the output image B in terms of their luminance, contrast and structure components and is calculated as follows:

$$\text{SSIM}(A,B) = \left(\frac{2\mu_A\mu_B}{\mu_A^2+\mu_B^2}\right)^a \left(\frac{2\sigma_A\sigma_B}{\sigma_A^2+\sigma_B^2}\right)^b \left(\frac{\sigma_{AB}}{\sigma_A\sigma_B}\right)^c \tag{23}$$

where

$$\mu_A = \frac{1}{L}\sum_{l=1}^{L} A_l$$

denotes the sample mean,

$$\sigma_A = \sqrt{\frac{1}{L-1}\sum_{l=1}^{L}(A_l-\mu_A)^2}$$

denotes the sample standard deviation and

$$\sigma_{AB} = \frac{1}{L-1}\sum_{l=1}^{L}(A_l-\mu_A)(B_l-\mu_B)$$

corresponds to the sample covariance calculated from their respective pixels A_l and B_l indexed as $l = 1, 2, \ldots, L$. In order to account for the higher relative importance of the contrast over the other two components of the measure, we set $a = c = 0.25$ and $b = 0.5$ in (23), thus giving more weight to the contrast measurement when calculating the SSIM in (23).

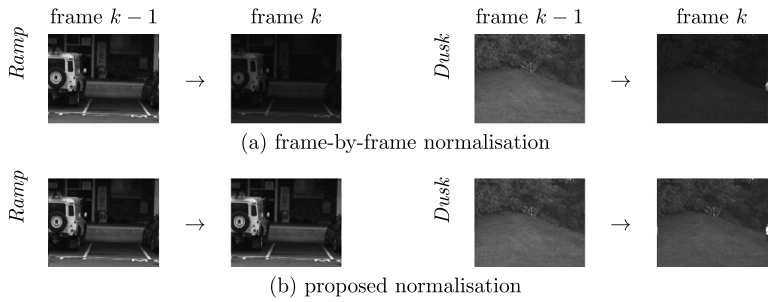

Fig. 5. Examples of the robust normalisation of a video, showing two subsequent video frames in two sequences. The change of dynamic range is caused by: the spark in the *Ramp* sequence and by a bright object (a person) entering the scene in the *Dusk* sequence. Note that while the standard normalisation (a) introduces flicker, the proposed normalisation (b) results in perceptually stable luminance.

3.2. Datasets

A mixture of general purpose and surveillance images has been used in our tests. Since SSIM-based quality metrics require a reference (i.e. a sufficiently illuminated image), the *Memorial*[2] and *Greenwich*[3] datasets, for which such an image is available, have been included in the tests. The remaining images, *Dusk*, *Ramp*, *Landrover* and *Doorway*, are taken from our multimodal surveillance image database[4] and represent a wide range of scenarios and lighting conditions.

3.3. Tested methods

The following methods have been used in our experiments: Image Stretching with 2% pixel saturation followed by gamma transformation of 0.85 ("IS-gamma"), Histogram Equalisation (HE), CLAHE [4,5,7] (a popular benchmarking method and a signification improvement over HE), our implementation of the wavelet domain enhancement method based on average local magnitude of coefficients [22] (in this correspondence referred to as Locally Adaptive Multiscale Contrast Optimisation (LAMCO) with gamma adjustment of 0.9), our implementation of contourlet-based[5] denoising and contrast enhancement method [33], Retinex[6] [53] and Brightness Preserving Dynamic Fuzzy Histogram Equalization (BPDFHE)[7] [54]. The competing methods have been chosen based on their reported good performance both in terms of enhancement and artefact introduction. It should be noted that in order to allow fair comparison, the pre-processing step (5) has been performed in all the tested CE methods, even if it has not been part of the original algorithm. Additionally, the images enhanced with LAMCO and Retinex method have been logarithmically scaled prior to the enhancement stage, as specified by the original algorithms.

3.4. Discussion of the results

Before images or video frames are transformed to the wavelet domain, the dynamic range normalisation of the data is performed and in case of video sequences time-dependent normalisation is applied as described in Section 2.2. The simulations performed with the use of image sequences from our dataset have shown that the improved temporal pre-processing appears to be perceptually smooth (see Fig. 5 for example results), at the expense of negligible saturation or under-scaling the video frame that may occasionally occur due to very abrupt dynamic range changes in a video.

The original and enhanced images obtained by applying the whole enhancement procedure (including pre- and post-processing) are shown in Figs. 6 and 7. We begin the subjective assessment of the results by observing that the test images enhanced by HE have a very bright, day light-like appearance. However, the amplification of the noise and saturation of the image pixels caused by HE led to a significant loss of some image detail (e.g. tree branches in *Landrover* or window details in *Memorial*) and introduction of artefacts (including artificial colours[8]). This is a significant drawback as it could contribute to confusion or increased false detections in the image when processed by a computer or presented to a human observer. Moreover, the loss of some image detail may result in less contextual information available in the enhanced image. The HE-type distortion is avoided when using CLAHE method at the expense of reduction in enhancement of low-energy image regions. The noise amplification still occurs, however to a smaller degree than in HE. Neither IS-gamma nor LAMCO enhancement introduce visible artefacts, but the enhanced images do not reveal the low-light information to a sufficient degree. While Retinex results in the strongest enhancement among the methods (in part due to the initial logarithmic scaling of the image), in many cases it results in white-washed output (e.g. in *Greenwich* image). Contourlet-based and BPDFHE methods enhance the images to a similar degree as LAMCO. The former method tends to over-emphasise the edges in the images which leads to a loss of the smoothness in the surfaces (e.g. in *Doorway* image) and the latter does not preserve the original colours in some cases (e.g. in *Landrover*). On the other hand, the proposed method does not introduce any visible distortion to the bright parts of the image but at the same time reveals sufficient detail in the dark parts of the image without amplifying the noise. Moreover, due to the optimisation being performed locally, the proposed method processes the low and high contrast regions of the image differently, enhancing certain regions of interest in the image to a greater extent than the other tested techniques. For example, the main challenge posed by the *Doorway* image is the shaded building entrance, contrasted with its well-illuminated surroundings. In this case, the image enhanced with the proposed method reveals a tube-shaped object in the entrance that the most of remaining methods fail to extract.

The numerical quality measure results given in Table 1 confirm that the proposed method achieves the best overall results

[2] Chris Tchou, Paul Debevec, HDR shop dataset, available at http://projects.ict.usc.edu/graphics/HDRShop, accessed September 2009.

[3] Aram Dulyan, Shutter speed in Greenwich, available at http://commons.wikimedia.org/wiki/File:Shutter_speed_in_Greenwich_(no_caption).jpg, accessed September 2009.

[4] The Eden project multi-sensor data set, http://www.imagefusion.org/, accessed November 2006.

[5] Contourlet toolbox accessed at http://www.ifp.illinois.edu/~minhdo/software/ has been used in this work.

[6] Retinex implementation, http://www.cs.sfu.ca/~colour/code/, accessed March 2013.

[7] BPFDHE implementation, http://www.mathworks.co.uk/matlabcentral/fileexchange/authors/207426, accessed March 2013.

[8] For interpretation of the references to color in this section, the reader is referred to the web version of this article.

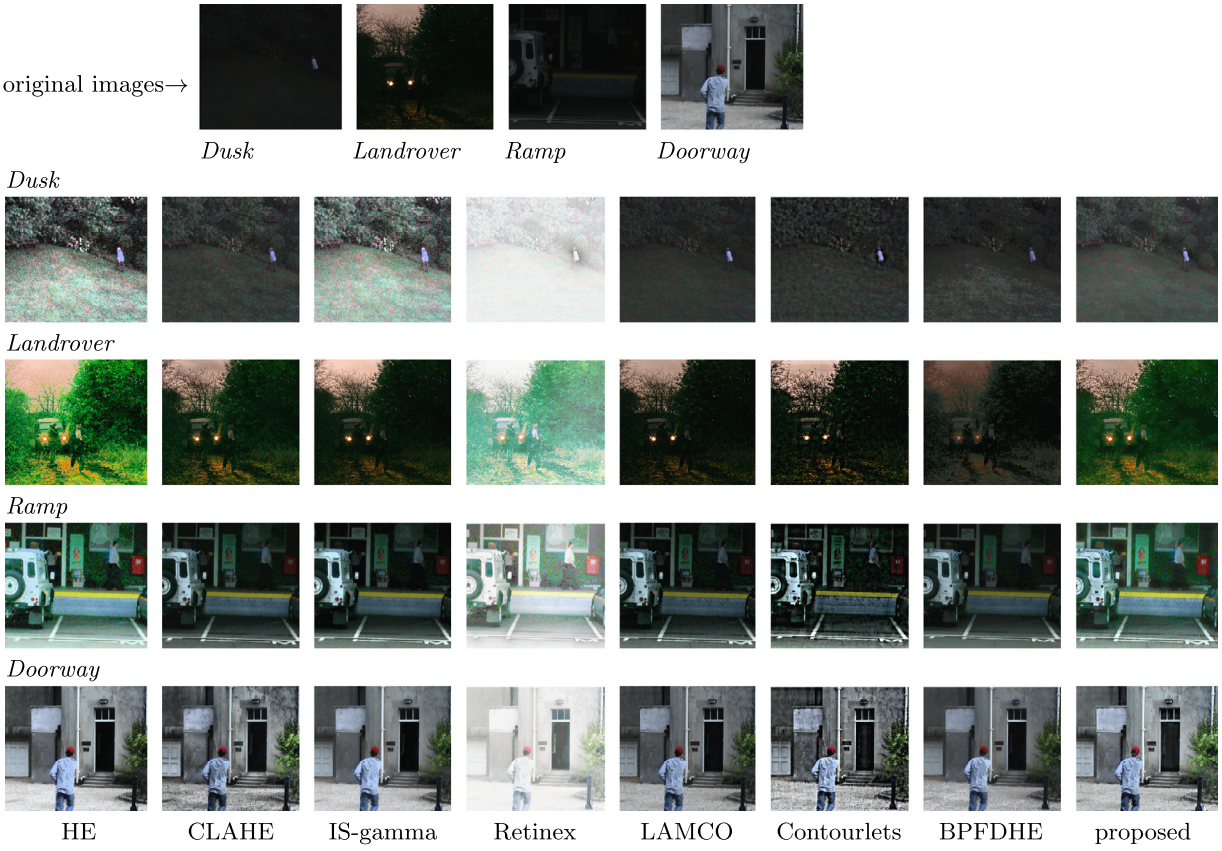

Fig. 6. The results of the image enhancement simulations.

Fig. 7. The results of the image enhancement simulations (datasets with reference images).

Table 1
Quality measurements of the enhancement methods.

Dataset	*Dusk*			*Landrover*			*Ramp*			*Doorway*			*Memorial*			*Greenwich*			
	$\hat{\sigma}_n^{(i)} = 2.53$			$\hat{\sigma}_n^{(i)} = 2.31$			$\hat{\sigma}_n^{(i)} = 1.40$			$\hat{\sigma}_n^{(i)} = 1.05$			$\hat{\sigma}_n^{(i)} = 0.59$			$\hat{\sigma}_n^{(i)} = 1.36$			
	$H^{(i)} = 4.08$			$H^{(i)} = 5.55$			$H^{(i)} = 5.04$			$H^{(i)} = 7.42$			$H^{(i)} = 4.98$			$H^{(i)} = 6.02$			
Metrics	$\hat{\sigma}_n^{(o)}$	S (%)	$H^{(o)}$	$\hat{\sigma}_n^{(o)}$	S (%)	$H^{(o)}$	$\hat{\sigma}_n^{(o)}$	S (%)	$H^{(o)}$	$\hat{\sigma}_n^{(o)}$	S (%)	$H^{(o)}$	$\hat{\sigma}_n^{(o)}$	S (%)	$H^{(o)}$	SSIM	$\hat{\sigma}_n^{(o)}$	S (%)	$H^{(o)}$	SSIM
HE	26.0	1.5	4.71	17.1	1.0	4.85	3.58	**0.0**	4.78	1.74	2.2	5.97	6.17	1.0	4.64	0.19	6.43	1.5	5.59	0.27
CLAHE	8.84	**0.0**	5.95	7.53	0.1	6.78	2.19	**0.0**	6.97	2.76	**0.0**	7.77	1.99	**0.1**	6.36	**0.67**	4.34	0.2	6.77	0.86
IS-gamm.	21.5	1.0	**7.79**	4.47	1.0	5.49	2.26	11.7	4.94	1.36	2.2	7.37	1.30	1.0	4.88	0.15	2.19	1.2	5.94	0.24
Retinex	5.03	1.2	5.42	12.37	0.6	**7.36**	3.32	0.3	7.51	**0.71**	0.3	6.64	3.42	0.3	**6.93**	0.62	2.50	0.5	6.15	0.82
LAMCO	4.55	**0.0**	5.41	3.35	2.7	6.08	1.96	3.4	7.08	1.24	0.5	7.67	0.77	0.5	5.58	0.53	1.10	1.1	6.44	0.85
Contour.	0.95	0.3	5.64	3.77	19.7	5.92	3.78	20.0	6.70	4.99	8.9	7.67	2.46	16.2	5.73	0.58	2.79	5.90	6.70	0.80
BPDFHE	4.07	**0.0**	5.38	3.9	1.1	5.11	1.46	**0.0**	5.91	1.15	0.1	7.33	1.07	**0.1**	4.95	0.52	2.14	**0.0**	6.30	0.82
proposed	**0.34**	0.1	5.92	**0.72**	0.6	7.02	**0.98**	1.6	**7.66**	0.91	2.0	**7.83**	**0.66**	0.5	6.81	0.66	**0.91**	1.0	**7.12**	**0.89**

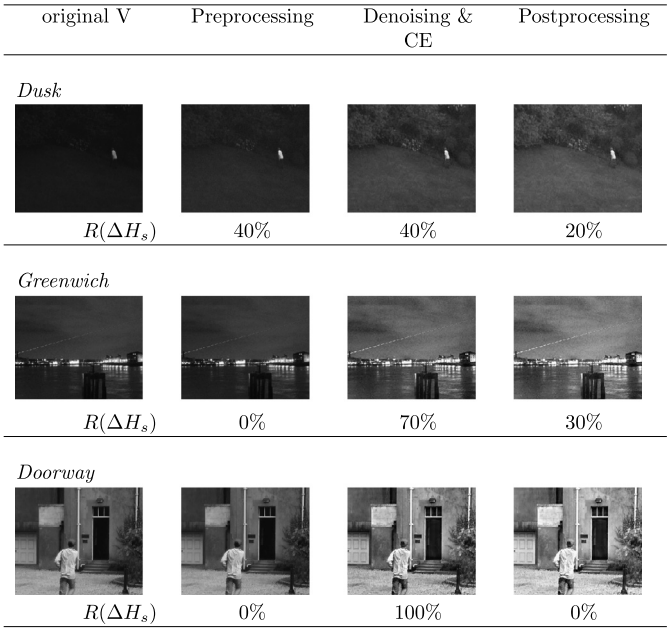

Fig. 8. The image enhancement results at subsequent stages of the proposed method.

in terms of noise reduction and contrast enhancement. Unlike the proposed method, all remaining methods increase the noise level in the output image and, in many cases, result in greater saturation of image pixels. Similarly, the proposed method results in the highest entropy among most of the images tested. The availability of the reference image in *Memorial* and *Greenwich* datasets, allows additional comparison. According to SSIM measurements the proposed method is the most similar to the reference *Greenwich* image and the second-best in terms of the similarity for *Memorial* image. In overall, the proposed method seems to offer the best trade-off between the degree of enhancement and introduction of artefacts among the methods tested, in a few particular cases being the second- or third-best.

As described in Section 2, the enhancement of the image is performed in three stages: (1) pre-processing, (2) enhancement, and (3) post-processing (see Fig. 1). In order to quantify the effect of subsequent modifications of the image, the relative entropy increments have been calculated at each stage of our enhancement procedure as follows

$$R(\Delta H_s) = \frac{H_s - H_{s-1}}{\mathrm{abs}(H^{(\mathrm{o})} - H^{(\mathrm{i})})} 100\%,$$

where $s = 1, 2, 3$ is the stage index; $H_0 = H^{(\mathrm{i})}$ is the input image entropy, and $H_3 = H^{(\mathrm{o})}$ is the entropy of the enhanced output image after applying the complete proposed procedure. Examples of the incremental enhancement are shown in Fig. 8 where it can be observed that the relative contribution of each stage depends on the dynamic range properties of the image in question. For example, the pre-processing procedure applied to *Dusk* image (the low dynamic range) corresponds to 40% of the overall entropy increment. On the other hand, for high dynamic range images such as *Greenwich* and *Doorway* the main contribution comes from the contrast enhancement stage that enhances the image locally. The $R(\Delta H_s)$ measurements performed on our dataset can be summarised as follows: the pre-processing accounts for 0–40%, contrast enhancement itself accounts for 40–100% and post-processing accounts for 0–30% of the overall enhancement, depending on the input image.

4. Conclusions

A method for contrast enhancement in low-light or unevenly illuminated images and videos has been proposed. The algorithm operates in the wavelet domain and re-scales the wavelet coefficients non-linearly based on their local dispersion. The enhancement methodology proposed does not require the user to specify or adjust parameters and is shown to work well with a range of general and surveillance imagery, outperforming both conventional and state-of-art methods, based on non-linear image stretch, gamma enhancement, histogram equalisation, Retinex and contourlet domain scaling in terms of feature extraction, enhancement, image quality, and noise reduction. When dealing with low-light video sequences, the proposed method stabilises the initial enhancement of video frames by introducing intensity normalisation based on the perceptual contrast discrimination threshold thus avoiding undesirable flicker in the enhanced video. It is also apparent that the images obtained with the proposed method are of better perceptional quality, compared to the methods tested. Specifically, the proposed enhancement results in sharper edges, brighter details in low-energy image regions and does not degrade the information in high-energy image regions.

Acknowledgment

The authors are grateful for the financial support offered to the project by General Dynamics UK Limited.

References

[1] E. Peli, Contrast in complex images, J. Opt. Soc. Amer. A 7 (10) (1990) 2032–2040, http://dx.doi.org/10.1364/JOSAA.7.002032.
[2] A. Beghdadi, A. Le Negrate, Contrast enhancement technique based on local detection of edges, Comput. Vis. Graph. Image Process. 46 (2) (1989) 162–174.
[3] R.C. Gonzalez, R.E. Woods, Digital Image Processing, Addison–Wesley Longman Publishing Co., Inc., Boston, MA, USA, 2008.
[4] K. Zuiderveld, Contrast limited adaptive histogram equalization, in: Graphics Gems IV, 1994, pp. 474–485.
[5] E.D. Pisano, S. Zong, B.M. Hemminger, M. DeLuca, R.E. Johnston, K.E. Muller, M.P. Braeuning, S.M. Pizer, Contrast limited adaptive histogram equalization image processing to improve the detection of simulated spiculations in dense mammograms, J. Digit. Imaging 11 (4) (1998) 193–200.
[6] F. Lamberti, B. Montrucchio, A. Sanna, CMBFHE: A novel contrast enhancement technique based on cascaded multistep binomial filtering histogram equalization, IEEE Trans. Consum. Electron. 52 (3) (2006) 966–974, http://dx.doi.org/10.1109/TCE.2006.1706495.
[7] A.M. Reza, Realization of the contrast limited adaptive histogram equalization (CLAHE) for real-time image enhancement, VLSI Signal Process. 38 (1) (2004) 35–44.
[8] Q. Wang, R. Ward, Fast image/video contrast enhancement based on weighted thresholded histogram equalization, IEEE Trans. Consum. Electron. 53 (2) (2007) 757–764, http://dx.doi.org/10.1109/TCE.2007.381756.
[9] R. Lakshmanan, M.S. Nair, M. Wilscy, R. Tatavarti, Automatic contrast enhancement for low contrast images: A comparison of recent histogram based techniques, in: International Conference on Computer Science and Information Technology, IEEE Computer Society, Los Alamitos, CA, USA, 2008, pp. 269–276.
[10] K. Panetta, E. Wharton, S. Agaian, Human visual system-based image enhancement and logarithmic contrast measure, IEEE Trans. Syst. Man Cybern. Part B: Cybern. 38 (1) (2008) 174–188, http://dx.doi.org/10.1109/TSMCB.2007.909440.
[11] T. Arici, S. Dikbas, Y. Altunbasak, A histogram modification framework and its application for image contrast enhancement, IEEE Trans. Image Process. 18 (9) (2009) 1921–1935, http://dx.doi.org/10.1109/TIP.2009.2021548.
[12] T. Celik, T. Tjahjadi, Contextual and variational contrast enhancement, IEEE Trans. Image Process. 20 (12) (2011) 3431–3441, http://dx.doi.org/10.1109/TIP.2011.2157513.
[13] M. Kaur, J. Kaur, J. Kaur, Survey of contrast enhancement techniques based on histogram equalization, Int. J. Adv. Comput. Sci. Appl. 2 (7) (2011) 137–141.
[14] T. Iwanami, T. Goto, S. Hirano, M. Sakurai, An adaptive contrast enhancement using regional dynamic histogram equalization, in: IEEE International Conference on Consumer Electronics, ICCE, 2012, pp. 719–722, http://dx.doi.org/10.1109/ICCE.2012.6162054.
[15] T. Celik, T. Tjahjadi, Automatic image equalization and contrast enhancement using Gaussian Mixture Modeling, IEEE Trans. Image Process. 21 (1) (2012) 145–156, http://dx.doi.org/10.1109/TIP.2011.2162419.
[16] X. Wu, A linear programming approach for optimal contrast-tone mapping, IEEE Trans. Image Process. 20 (5) (2011) 1262–1272, http://dx.doi.org/10.1109/TIP.2010.2092438.
[17] C. Gao, K. Panetta, S. Agaian, A new color contrast enhancement algorithm for robotic applications, in: 2012 IEEE International Conference on Technologies for Practical Robot Applications, TePRA, 2012, pp. 42–47, http://dx.doi.org/10.1109/TePRA.2012.6215652.
[18] J. Short, J. Kittler, K. Messer, A comparison of photometric normalisation algorithms for face verification, in: Proceedings of the Sixth IEEE International Conference on Automatic Face and Gesture Recognition, 2004, pp. 254–259, http://dx.doi.org/10.1109/AFGR.2004.1301540.
[19] A. Jimenez-Sanchez, J. Mendiola-Santibanez, I. Terol-Villalobos, G. Herrera-Ruiz, D. Vargas-Vazquez, J. Garcia-Escalante, A. Lara-Guevara, Morphological background detection and enhancement of images with poor lighting, IEEE Trans. Image Process. 18 (3) (2009) 613–623, http://dx.doi.org/10.1109/TIP.2008.2010152.
[20] J.-L. Starck, F. Murtagh, E. Candes, D. Donoho, Gray and color image contrast enhancement by the curvelet transform, IEEE Trans. Image Process. 12 (6) (2003) 706–717, http://dx.doi.org/10.1109/TIP.2003.813140.
[21] Q. Li, X. Ni, G. Liu, Ceramic image processing using the second curvelet transform and watershed algorithm, in: IEEE International Conference on Robotics and Biomimetics, ROBIO, 2007, pp. 2037–2042, http://dx.doi.org/10.1109/ROBIO.2007.4522481.
[22] N. Bonnier, E. Simoncelli, Locally adaptive multiscale contrast optimization, in: IEEE International Conf. on Image Processing, vol. 1, ICIP, 2005, pp. I-949–I-952, http://dx.doi.org/10.1109/ICIP.2005.1529909.
[23] J. Tang, E. Peli, S. Acton, S. Member, S. Member, Image enhancement using a contrast measure in the compressed domain, IEEE Signal Process. Lett. 10 (2003) 289–292.
[24] J. Lu, D. Healy, Contrast enhancement via multiscale gradient transformation, in: Proceedings of IEEE International Conference on Image Processing, vol. 2, ICIP-94, 1994, pp. 482–486, http://dx.doi.org/10.1109/ICIP.1994.413617.
[25] X. Zong, A. Laine, E. Geiser, Speckle reduction and contrast enhancement of echocardiograms via multiscale nonlinear processing, IEEE Trans. Med. Imag. 17 (4) (1998) 532–540, http://dx.doi.org/10.1109/42.730398.
[26] S. Nercessian, S.S. Agaian, K.A. Panetta, Multi-scale image enhancement using a second derivative-like measure of contrast, in: Image Processing: Algorithms and Systems X; and Parallel Processing for Imaging Applications II, Proc. SPIE 8295 (2012), http://dx.doi.org/10.1117/12.906494, article 82950Q, 9 pp.
[27] J. Lu, D.M. Healy Jr., J.B. Weaver, Contrast enhancement of medical images using multiscale edge representation, Opt. Eng. 33 (07) (1994) 2151–2161.
[28] H. Kaiqi, W. Zhenyang, W. Qiao, Image enhancement based on the statistics of visual representation, Image Vis. Comput. 23 (1) (2005) 51–57, http://dx.doi.org/10.1016/j.imavis.2004.07.005.
[29] A. Mencattini, F. Caselli, M. Salmeri, R. Lojacono, Wavelet based adaptive algorithm for mammographic images enhancement and denoising, in: Proceedings ICIP-05 (IEEE International Conference on Image Processing), vol. 1, 2005, pp. I-1141–I-1144, http://dx.doi.org/10.1109/ICIP.2005.1529957.
[30] D. Heric, B. Potocnik, Image enhancement by using directional wavelet transform, in: 28th International Conference on Information Technology Interfaces, 2006, pp. 201–206, http://dx.doi.org/10.1109/ITI.2006.1708478.
[31] E. Nezhadarya, M. Shamsollahi, Image contrast enhancement by contokeywordset transform, in: 48th International Symposium ELMAR-2006 focused on Multimedia Signal Processing and Communications, 2006, pp. 81–84, http://dx.doi.org/10.1109/ELMAR.2006.329520.
[32] M. Asmare, V. Asirvadam, L. Iznita, Multi-sensor image enhancement and fusion for vision clarity using contokeywordset transform, in: International Conference on Information Management and Engineering, ICIME'09, 2009, pp. 352–356, http://dx.doi.org/10.1109/ICIME.2009.112.
[33] K. Li, X. Chen, X. Hu, X. Shi, L. Zhang, Image denoising and contrast enhancement based on nonsubsampled contourlet transform, in: 2010 3rd IEEE International Conference on Computer Science and Information Technology (ICCSIT), vol. 2, 2010, pp. 131–135, http://dx.doi.org/10.1109/ICCSIT.2010.5563631.
[34] A. Toet, Multiscale contrast enhancement with applications to image fusion, Opt. Eng. 31 (1992) 1026–1031, http://dx.doi.org/10.1117/12.56155.
[35] T. Jinno, K. Mouri, M. Okuda, HDR video tone mapping based on gamma blending, in: Proceedings of International Conference on Image Processing, 2010, pp. 2521–2524, http://dx.doi.org/10.1109/ICIP.2010.5649210.
[36] G. Krawczyk, K. Myszkowski, H.-P. Seidel, Perceptual effects in real-time tone mapping, in: Proceedings of the 21st Spring Conference on Computer Graphics, SCCG'05, ACM, New York, NY, USA, 2005, pp. 195–202, http://dx.doi.org/10.1145/1090122.1090154.
[37] D.F. Rogers, Procedural Elements of Computer Graphics, 2nd ed., McGraw–Hill, 1997.
[38] R. Mantiuk, K. Myszkowski, H.-P. Seidel, A perceptual framework for contrast processing of high dynamic range images, ACM Trans. Appl. Percept. 3 (3) (2006) 286–308, http://doi.acm.org/10.1145/1166087.1166095.
[39] P. Whittle, Increments and decrements: Luminance discrimination, Vis. Res. 26 (10) (1986) 1677–1691, http://dx.doi.org/10.1016/0042-6989(86)90055-6.

[40] N.G. Kingsbury, Image processing with complex wavelets, Philos. Trans. R. Soc. Lond. Ser. A Math. Phys. Eng. Sci. 357 (1999) 2543–2560.
[41] N.G. Kingsbury, Complex wavelets for shift invariant analysis and filtering, Appl. Comput. Harmon. Anal. 10 (2001) 234–253.
[42] P. Hill, N. Canagarajah, D. Bull, Image fusion using complex wavelets, in: Proc. 13th British Machine Vis. Conf., BMVC-2002, 2002, pp. 487–496.
[43] A. Achim, A. Loza, D.R. Bull, C.N. Canagarajah, Statistical modelling for wavelet domain image fusion, in: T. Sthathaki (Ed.), Image Fusion: Theory and Applications, Academic Press, 2008, pp. 119–138.
[44] A. Loza, D. Bull, N. Canagarajah, A. Achim, Non-Gaussian model-based fusion of noisy images in the wavelet domain, Comput. Vis. Image Underst. 114 (1) (2010) 54–65.
[45] G. Samorodnitsky, M.S. Taqqu, Stable Non-Gaussian Random Processes: Stochastic Models with Infinite Variance, Chapman and Hall, New York, 1994.
[46] C.L. Nikias, M. Shao, Signal Processing with Alpha-Stable Distributions and Applications, John Wiley and Sons, 1995.
[47] A. Achim, D. Herranz, E. Kuruoglu, Astrophysical image denoising using bivariate isotropic Cauchy distributions in the undecimated wavelet domain, in: Proceedings of International Conference on Image Processing, vol. 2, 24–27 Oct. 2004, pp. 1225–1228, http://dx.doi.org/10.1109/ICIP.2004.1419526.
[48] R. Coifman, D. Donoho, Time-invariant wavelet denoising, in: A. Antoniadis, G. Oppenheim (Eds.), Wavelet and Statistics, in: Lecture Notes in Statist., vol. 103, Springer-Verlag, 1995, pp. 125–150.
[49] P.J. Huber, Robust estimation of a location parameter, Ann. of Math. Stat. 35 (1) (1964) 73–101.
[50] C. Shannon, A mathematical theory of communication, Tech. Rep., Bell Syst. Tech. J. 27 (1948) 379.
[51] Z. Wang, A. Bovik, H. Sheikh, E. Simoncelli, Image quality assessment: From error visibility to structural similarity, IEEE Trans. Image Process. 13 (4) (2004) 600–612.
[52] C. Thum, Measurement of the entropy of an image with application to image focusing, Opt. Acta 31 (1984) 203–211, http://dx.doi.org/10.1080/713821475.
[53] B. Funt, F. Ciurea, J. McCann, Retinex in matlab, in: Proceedings of the IS&T/SID Eighth Color Imaging Conference: Color Science, Systems and Applications, 2000, pp. 112–121.
[54] D. Sheet, H. Garud, A. Suveer, M. Mahadevappa, J. Chatterjee, Brightness preserving dynamic fuzzy histogram equalization, IEEE Trans. Consum. Electron. 56 (4) (2010) 2475–2480, http://dx.doi.org/10.1109/TCE.2010.5681130.

Artur Łoza received his M.Sc. degree from Wroclaw University of Technology, Poland and a Ph.D. degree from the University of Bristol, UK. In 2004 he has joined University of Bristol as a Research Associate, where he currently holds the position of a Visiting Research Fellow. During 2007–2008 he has spent several months as a Visiting Researcher at Universidad Carlos III de Madrid, Spain. In 2010 he has been awarded EU-funded 2-years postdoctoral fellowship to conduct his research at the Shanghai Jiaotong University, China. He is currently with Khalifa University of Science, Technology and Research, UAE, as a Postdoctoral Fellow. His main areas of research are: multi-resolution and statistical image processing, image enhancement, multimodal image fusion and video object tracking. He has co-authored over 20 scientific publications.

David R. Bull (PhD, FIET, FIEEE, CEng) received the B.Sc. degree from the University of Exeter, Exeter, UK, in 1980, the M.Sc. degree from the University of Manchester, Manchester, UK, in 1983, and the Ph.D. degree from the University of Cardiff, Cardiff, UK, in 1988.His previous roles include: Lecturer at the University of Wales (Cardiff) and Systems Engineer for Rolls Royce. He was Head of the Electrical and Electronic Engineering Department at Bristol between 2001 and 2006 and is now Director of the Bristol Vision Institute (BVI). In 2001, he co-founded ProVision Communication Technologies, Ltd. He has worked widely in the fields of 1-D and 2-D signal processing. He has won two IEE Premium awards for this work and has published numerous patents, several of which have been exploited commercially. His current activities are focused on the problems of image and video communications and analysis for wireless, internet, surveillance, and broadcast applications. He has published some 400 academic papers, various articles and two books and has also given numerous invited/keynote lectures and tutorials.

Paul R. Hill received his B.Sc. degree from the Open University, a M.Sc. degree from the University of Bristol, Bristol, UK and a Ph.D. also from the University of Bristol. He is currently a Research Fellow at the University of Bristol and part time lecturer. His research interests include image and video analysis, compression and fusion. He has published over 20 academic papers.

Alin M. Achim received the B.Sc. and M.Sc. degrees, both in electrical engineering, from University “Politehnica” of Bucharest, Romania, in 1995 and 1996, respectively and the Ph.D. in biomedical engineering from the University of Patras, Greece, in 2003. He then obtained an ERCIM (European Research Consortium for Informatics and Mathematics) postdoctoral fellowship which he spent with the Institute of Information Science and Technologies (ISTI-CNR), Pisa, Italy and with the French National Institute for Research in Computer Science and Control (INRIA), Sophia Antipolis, France. In October 2004 he joined the Department of Electrical & Electronic Engineering at the University of Bristol as a Lecturer. He became Senior Lecturer in 2010. His research interests are in statistical signal, image and video processing, multi-resolution algorithms, wavelet analysis of digital images, image filtering and fusion, segmentation and classification. He has co-authored over 80 scientific publications, is an editorial board member of Digital Signal Processing (Elsevier), and has served on numerous conferences technical programme committees in signal and image processing. Alin has been organising committee member of the International Conference on Biosensing Technologies (Bristol 2009, Amsterdam 2011 and Barcelona 2013), of the Biomedical Imaging Workshop (Bristol 2010), and of the INGIMED X Conference (Bucharest 2009). He is member of the IET and a Senior Member of the IEEE.